Faraday Discussions

Cite this: DOI: 10.1039/d5fd00156k

PAPER

Probing interfacial vibrations with IR absorption spectroscopy: from molecular to mesoscopic and macroscopic surfaces

Ashley M. Stingel, [a] Bashar Moussa, [a] Lilian Najm Alsayed, [a] Dennis K. Hore [b] and Poul B. Petersen *[a]

Received 8th December 2025, Accepted 26th February 2026
DOI: 10.1039/d5fd00156k

Capturing the vibrational signatures of interfacial molecules is complicated by their low abundance relative to bulk molecules. Molecules at extended flat liquid interfaces can be elegantly singled out and probed by vibrational sum-frequency generation (SFG) spectroscopy as this method is intrinsically surface-specific due to the requirement of broken inversion symmetry. Interfacial molecules in solvation shells at molecular interfaces, on the other hand, exhibit inversion symmetry and vanish in SFG spectroscopy. However, in several cases, the fraction of solvent molecules at such molecular interfaces can be several percent of the total and can be isolated using advanced subtraction methods. Raman-MCR spectroscopy was first developed as a general and accurate method for extracting the Raman spectrum of this fraction of solvent molecules in the solvation shells of solutes. We later adapted the technique to FTIR spectroscopy in the form of ATR spectroscopy. The method is, in essence, a difference spectroscopy, wherein the vibrational spectrum of a solution is considered to be composed of two contributions: (i) that of the bulk solvent, which can be either a pure liquid or a mixture itself, and (ii) that of the solute with its solvation shell, defined as the part of the solvent that is perturbed by the interactions with the solute. In solvation shell spectroscopy, the bulk solvent contribution is removed from the solution spectrum, and the solute-correlated spectrum is then obtained. This solute-correlated spectrum contains the vibrational modes of the solute itself and those of perturbed molecules at the solute–solvent interface, which can reveal information such as the strength and extent of solute–solvent interactions. Here, we discuss advantages and complications of the method in detail using *tert*-butyl alcohol, a small amphiphilic molecule, as an example, starting in pure water and moving to more complex systems including ionic additives and mixed solvents. We furthermore illustrate how changes in the hydrogen-bond strength in the solvent shell can be quantified. Lastly, we push the spectroscopy to the detection limit and show that solvent interactions can be probed at not only molecular interfaces, but also meso- and even macroscopic interfaces. When done correctly, solvation

[a]*Faculty of Chemistry and Biochemistry, Ruhr-University Bochum, 44801 Bochum, Germany. E-mail: poul.petersen@ruhr-uni-bochum.de*
[b]*Department of Chemistry, University of Victoria, Victoria, British Columbia V8W 3 V6, Canada*

shell spectroscopy holds great promise to be widely implemented to study solvent interactions in a wealth of different simple and complex systems.

Introduction

Interfaces are omnipresent. Here, molecules come together and react. In principle, all chemical reactions take place at an interface. Interfaces come in many chemical and physical forms, ranging from flat macroscopic interfaces between different phases, such as solid–air, liquid–air, solid–liquid, *etc.*; to the surfaces of meso-scaled objects, such as nanometer- to micron-sized bubbles, droplets, and beads; and to molecular interfaces ranging from large biomolecules to small solutes. All of these interfaces have in common that the solvent is perturbed due to the different interactions between the chemical nature of the interface and the solvent molecules compared with solvent–solvent interactions. For the most part in this discussion, we consider the solvent to be pure water, aqueous solutions (buffers), or water–alcohol mixtures. In such aqueous solvents, the hydrogen-bonding interactions between the interfacial molecules and the water molecules dominate the interaction. Since the hydrogen-bond interactions with the interface are different than the hydrogen-bond interactions between solvent water molecules, the structure of the interfacial solvent is different than that of the bulk solvent, and this structural difference directly reflects the solvent–interface interaction. Vibrational spectroscopy is an excellent probe of the aqueous solvent structure due to the close relationship between the frequency of the OH stretch and the strength of the hydrogen bond.[1–3] However, capturing the vibrational spectrum of the interfacial solvent molecules is notoriously difficult given the low number of molecules present in interfacial layers relative to the bulk.

For flat macroscopic interfaces, nonlinear spectroscopy in the form of sum-frequency generation (SFG) has, over the last three decades, become a powerful method for capturing the vibrational spectrum of interfacial molecules.[4–9] Here, the requirement of broken inversion symmetry within the dipole approximation ensures that the signal measured comes only from the interfacial molecules. Consequently, SFG is a background-free method – any photons generated at the sum of the incident photon energies come from the interface. As a consequence, SFG can be used to obtain the vibrational spectrum of macroscopic flat interfaces and chiral structures, as chirality also breaks inversion symmetry.[10,11] For meso-scale objects such as micron-sized droplets or beads, the scattering version of SFG, sum-frequency scattering (SFS), can be used to probe the vibrations at the surfaces of the particles in solution.[12,13] However, as nonlinear optical methods, SFG and SFS require advanced laser systems and typically result in weak signals with a corresponding relatively small signal-to-noise ratio (S/N). Experimental setups for these nonlinear experiments are typically home-built with varying degrees of user-friendliness, although commercial spectrometers have entered the market.

While SFG and SFS are not sensitive to molecules at molecular interfaces, as the net interactions remain isotropic, these can be probed by linear spectroscopy. For solutions, bulk-allowed methods such as spontaneous Raman scattering and IR absorption spectroscopy typically focus on vibrations of the solute molecules since the contribution of surface-perturbed solvent molecules, including those in

the solvation shells of the solute, is overwhelmed by the bulk solvent. However, in some systems, the contribution from interfacial solvent molecules can be several percent of the total signal and, through careful experimental design, this surface contribution can be extracted. This relies on high data quality with good spectral resolution and, more importantly, an excellent signal-to-noise ratio, which is readily attainable with IR and Raman spectroscopy. There is a long history of so-called difference spectroscopy, where a reference spectrum is carefully subtracted from the spectrum of interest to reveal features that would otherwise not be apparent. Multivariate curve resolution (MCR) is an alternative to weighted subtraction that can have some performance advantages. The most common utilization of difference spectroscopy is to remove the effects of water to better observe, or to more quantitatively analyze, vibrational modes of other species.[14–17] However, for our present interest, we focus on the subset of those methods that seek to isolate interfacial water signals.[18–21] As we will describe in more detail here, this requires an extremely careful control of the experimental geometry and a high level of accuracy in the subtraction, as we seek to uncover often subtle differences between the hydrogen-bonding environments of bulk water and water at interfaces such as solvation shells. Solvation shell spectroscopy has been extensively explored using Raman spectroscopy, including the use of MCR.[18–30] When it comes to IR absorption, attenuated internal reflection (ATR-IR) offers the possibility to limit the penetration depth of the light in the aqueous phase, which limits distortions due to the high absorbance of water and, in some cases, can assist in achieving better contrast in difference spectroscopy.

Surface-enhanced IR absorption spectroscopy (SEIRAS), including in an ATR configuration, is another means by which the spectral features of surface water can be enhanced relative to bulk water.[31–35] A related technique that draws on developments in the plasmonics community is shell-isolated nanoparticle-enhanced Raman spectroscopy (SHINERS), where metal nanoparticles are deposited onto planar metal interfaces for additional electric field localization.[36–38] While those methods have demonstrated excellent results, particularly for electrode surfaces, we are interested in techniques that can be used to study dielectric surfaces and other non-metal interfaces in solution. In theory, IR-based methods should offer a signal-to-noise advantage over Raman, and that is critical to the fidelity of the difference spectroscopy. Inspired by this, we applied the Raman-MCR approach originally proposed by Ben-Amotz to FTIR spectroscopy utilizing attenuated total reflectance (ATR).[39] We have recently extended the method to examine a number of different systems studying both the molecules at the interface of the ATR crystal and the molecular interface in liquid solutions.[40–42] Here, we describe the method in detail taking the small amphiphilic molecule *tert*-butyl alcohol as an illustrative example. We show how solvation shell spectroscopy can not only be applied to pure solvents (water) but also to quantify the amount of ions in the solvation shell in ionic solutions, to characterize the solvent composition in mixed solvents, and furthermore to quantify the hydrogen-bonding interactions in the solvation shell. We illustrate that using a weighted subtraction provides the same results as using the MCR method but has advantages at low concentrations, where the signal-to-noise ratio (S/N) is worse. Given this, we show that, ultimately, solvation shell spectroscopy can not only be applied to molecular interfaces, but also to mesoscopic objects in the form of micron-sized beads, and even to macroscopically flat interfaces.

Careful consideration of crystal elements, proper cleaning, and purging of the setup are needed to perform solvation shell spectroscopy, but when done meticulously, solvent interactions can be studied in practically any system, including small molecules, biomolecules, solvent additives, solvent mixtures, macroscopic beads, membrane surfaces, and other complex systems.

Methods

Solvation shell spectroscopy

In the dilute limit, a solution can be considered as a two-component system: (i) the solute itself together with its solvation shell, defined as the part of the solvent that is perturbed by the solute, and (ii) the bulk solvent. The fundamental principle of solvation shell spectroscopy is to remove the bulk solvent contribution to the total spectrum, leaving behind the solute-correlated spectrum, *i.e.*, the part of the spectrum that cannot be attributed to the bulk solvent, containing the spectrum of the solute itself and the perturbed solvent in the solvent shell. This is achieved by measuring the spectrum of the solution and that of the pure solvent. In the simplest case, this is the spectrum of the aqueous solution and that of pure water, but the same method can be applied to more complex systems, as described later. The solvation shell spectrum is obtained by simply subtracting the bulk solvent component from the total spectrum after scaling it with a subtraction factor (α), as illustrated in Fig. 1, leaving only vibrations that are different from those of the bulk solvent – those belonging to the solute with its solvation shell. The subtraction factor accounts for the fact that the solute with solvation shell occupies a fraction of the total sample volume. If the volume of the solute and its solvation shell is 5%, then the subtraction factor would be 0.95, corresponding to the reduced effective volume of the bulk solvent. The traditional approach of measuring a pure solvent background spectrum would correspond to having a subtraction factor of 1 and give rise to negative solvent peaks, since the solution contains less solvent overall than in the pure solvent. The key is to find the correct subtraction factor – while the effective volume of the solute itself can

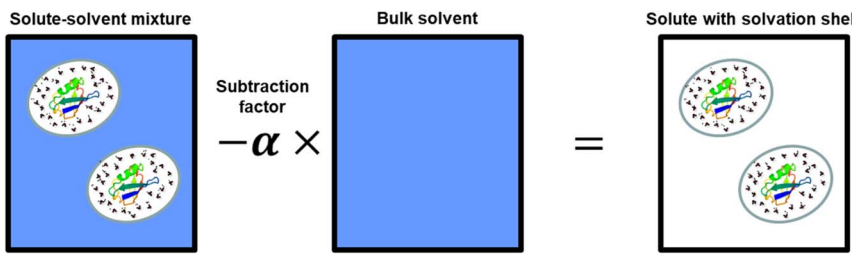

Fig. 1 Principle of solvation shell spectroscopy. IR solvation shell spectroscopy is, in principle, a subtraction method, where the total spectrum of a solution is considered to have two components: the solute with its solvation shell and the bulk solvent. The spectrum of the solute with its solvation shell is obtained by subtracting the contribution from the bulk solvent. This is obtained by scaling the spectrum of the bulk solvent with a factor α to account for the volume occupied by the solute and solvation shell to obtain the least non-negative spectrum, *i.e.*, the solute-correlated spectrum or simply "the solvation shell spectrum".

be determined experimentally, the volume including the solvation shell cannot be determined independently. This is critical to separating the dominating bulk-like solvent spectrum from the substantially smaller contributions of solvent molecules perturbed by the solute, and relies on the fact that absorption spectra are positive quantities. This means that the solvation shell spectrum is found using the highest value of α without any part of the spectrum being negative – the least non-negative spectrum. In other words, the coefficient is gradually increased until any part of the subtracted spectrum becomes negative, thus removing all of the bulk contribution from the total spectrum and leaving only the part of the spectrum that is unique to the solute: the solute-correlated spectrum, which contains the spectrum of the solute itself and that of the solvent, which is spectrally shifted due to the solute–solvent interactions. The MCR routines find the mathematically rigorous least non-negative spectrum. However, due to experimental noise and background fluctuations, these are not necessarily the optimal spectral results and require optimization of the subtraction constant, also referred to as rotation of the basis set. This is discussed in further detail below.

ATR spectroscopy

Solvation shell spectroscopy relies on the additivity of spectral components and thus requires that Beer's Law be obeyed. While this is not a problem in Raman spectroscopy given the low cross-section of the Raman scattering probability, this is a considerable limitation in IR spectroscopy. In a normal transmission experiment, the OH-stretch band of water saturates for all but the very thinnest transmission cells. Even in a 25 μm-thick cell, for example, the absorbance of the OH stretch is more than 10. This limitation can be overcome using attenuated total reflectance (ATR), where the effective pathlength is typically on the order of 1 μm or less. The effective pathlength is dependent on both the penetration depth of the field into the liquid solution, on the local field factors, and on the number of bounces in the internal reflecting element (IRE) of the ATR setup. The effective pathlength in ATR-FTIR spectroscopy is wavelength-dependent and central to the solvation shell method, and further depends on the choice of crystal and geometry, which are important considerations and are discussed in detail in the SI. Furthermore, as a subtraction method, solvation shell spectroscopy requires a large signal-to-noise (S/N) ratio and is very sensitive to baseline fluctuations, contaminations, and interferences due to light absorption by atmospheric molecules, most notably water and CO_2. In its simplicity, solvation shell spectroscopy is deceptively straightforward, but when not applied with care, such effects can lead to artifacts and misinterpretations. The SI also includes a discussion of how to avoid artifacts and obtain high-quality solvation shell spectra.

Results and discussion

Raman *vs.* IR-ATR solvation shell spectroscopy

Most systems that are considered are aqueous solutions. Water is a particularly interesting system given the sensitivity of the OH stretch to the hydrogen-bond strength.[1–3] Here, an isolated non-hydrogen-bonded OH, also referred to as a free OH, gives rise to a narrow band at around 3700 cm^{-1} in the spectrum. Upon

hydrogen bonding, the OH stretch shifts to lower frequencies as a function of the hydrogen-bond strength and broadens as the hydrogen-bond interactions weaken the OH bond and widen the potential. This is a well-known correlation that can shift the OH stretch all the way down to 1000 cm^{-1} for very strong hydrogen-bonded systems.[43] Since the OH stretch is particularly sensitive to hydrogen-bond interactions, the water molecules in the solvation shell of the solute are spectrally shifted depending on the difference in the interactions between solute and water compared with the interactions between bulk water molecules. This shift can be to either higher or lower frequencies relative to bulk water, depending on the relative hydrogen-bond interactions between solute and solvent compared with those in bulk water.

The water OH stretch and bend vibrations, which are typically the focus of solvation shell spectroscopy, are both IR and Raman allowed, making the two approaches to solvation shell spectroscopy similar. However, there are other noteworthy differences between IR and Raman given the differences in selection rules of other vibrations. For instance, the CH-stretch vibrations of the solute are typically much stronger, relative to the OH stretch, in Raman than in IR. This can complicate the analysis of strongly hydrogen-bonded OH vibrations since they can overlap with the CH-stretch vibrations. On the other hand, while the oscillator strength of the OH stretch varies in the IR, the scattering probability in Raman is fairly flat across the spectrum.[2,3] This means that the free OH is typically more pronounced in Raman solvation shell spectroscopy than in the IR analogue. Raman solvation shell spectroscopy thus has advantages when characterizing the free-OH vibrations and quantifying the number of perturbed water molecules, while IR solvation shell spectroscopy has advantages when characterizing strongly hydrogen-bonded species. Depending on the specific sample, ATR spectroscopy can exhibit a higher sensitivity, making it possible to operate at lower concentrations. However, the presence of the crystal in ATR spectroscopy can cause problems with surface aggregation and care must be taken in cleaning the crystal, as discussed in the SI. IR-ATR and Raman solvation shell spectroscopies thus offer complementary strengths. In most cases, either IR-ATR or Raman solvation shell spectroscopy is sufficient to characterize the system of interest, but given the differences in selection rules, combining the methods can be advantageous, as illustrated by combined IR and Raman solvation shell studies, combined with theoretical calculations, that shed light on the intricate nature of the excess proton and proton shuttling in water under acidic conditions,[44] and on water–hydroxide interactions and proton shuttling in basic solutions.[45]

Solvation shell spectroscopy *via* weighted subtraction

In the pioneering work by Ben-Amotz and coworkers, MCR routines were used to extract the solute-correlated spectra from the Raman spectra of solutions.[18–21] In our earlier works on IR solvation shell spectroscopy, we also applied the same routine, as provided by the Ben-Amotz group. Such MCR routines find the mathematically rigorous least-positive solute-correlated spectrum – that is, the largest extraction coefficient without any part of the spectrum becoming negative. However, this does not account for experimental noise and baseline drifts. For instance, the MCR routine finds the solution where the lowest noise spike in the solvation shell spectrum is zero, and not the more experimentally reasonable

solution, where the noise is centred around zero. Therefore, after finding the mathematically rigorous solution with MCR, the optimal solvation shell spectrum is then fine-tuned by rotating the basis set.

More recently, we have instead applied a weighted subtraction method. Ben-Amotz and co-workers previously compared these approaches and found that the methods are equivalent in Raman spectroscopy for two-component systems.[46] IR-ATR spectroscopy exhibits different imperfections, such as baseline drifts and atmospheric interferences, compared with Raman spectroscopy, which can influence the analysis. These imperfections are typically not significant at higher solute concentrations, but become important at lower concentrations or for extensions to mesoscale and macroscopic systems, which inherently have lower S/N due to the smaller surface-to-bulk ratio. Below, we compare the methods and provide several examples of IR solvation shell spectroscopy of increasingly complex systems. These results demonstrate the usefulness of the method with smaller signals, allowing extensions to increasingly complex systems as well as mesoscale and macroscopic interfaces discussed below.

TBA: the fruit fly of solvation shell spectroscopy. *Tert*-butyl alcohol (TBA) is a convenient test molecule for solvation shell spectroscopy. This amphiphilic molecule is particularly informative as it contains both a hydrogen-bond-breaking hydrophobic region and a hydrogen-bond-forming OH group. The Ben-Amotz group studied TBA with Raman-MCR spectroscopy to reveal information on its solvation, aggregation, and interactions with other small solutes.[19,47–50] Accordingly, it was also an important demonstration in our first application.[39] Here, we demonstrate solvation shell spectroscopy, including its applications and limitations, first on aqueous solutions of TBA at high and low concentrations and then on increasingly complex multi-component systems.

Initial processing of the data. The raw IR-ATR spectrum is initially processed to remove offsets and correct for the frequency-dependent penetration depth, as described in the SI. In the multi-bounce germanium ATR, the effective pathlength (ℓ_e) varies from 3.99 μm at 1000 cm^{-1} to 0.9 μm at 4000 cm^{-1}. This results in an exaggerated OH bend ($\ell_e \approx 2.3$ μm) relative to the OH stretch ($\ell_e \approx 1.1$ μm) in aqueous samples, compared with a transmission experiment. Correcting for this frequency-dependent pathlength normalizes the spectrum to absorbance per μm, *i.e.*, makes the absorbance equivalent to that measured in a transmission cell with a thickness of 1 μm.

Weighted subtraction. Obtaining the solvation shell spectrum of TBA *via* the weighted subtraction method is demonstrated in Fig. 2, showing both gross and fine adjustments of the scalar α. We find it useful to initially purposely slightly oversubtract the solvation shell spectrum to highlight the differences relative to the bulk spectrum. The most extreme case, $\alpha = 1$, shown in Fig. 2a, results in the direct difference spectrum – the solution minus the solvent – with negative peaks corresponding to the solvent peaks. This is equivalent to blanking the spectrometer with the pure solvent. As described above, this occurs because as the solute occupies volume, the solvent volume is reduced and, in effect, oversubtracted. In particular, this overwhelms the OH-stretch contributions of the solute. By reducing α until there is no negative signal remaining, we remove only the effective amount of bulk solvent in the solution, leaving behind the spectrum of the solute and any solvent molecules that are no longer "bulk-like".

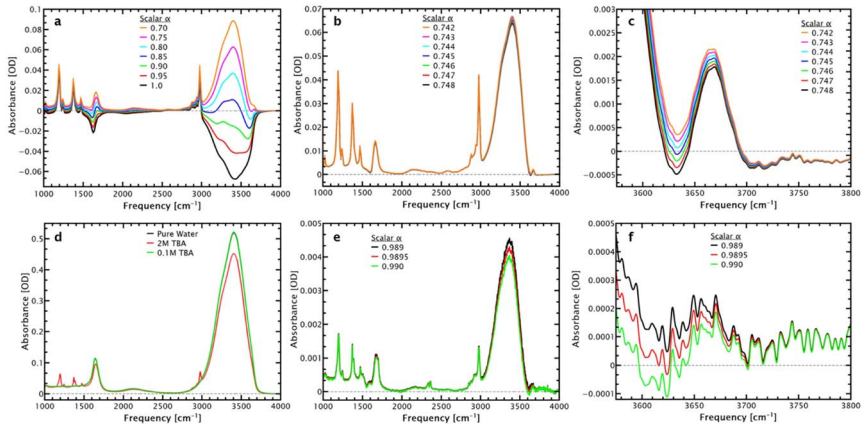

Fig. 2 The solvation shell spectrum of TBA obtained *via* the weighted subtraction method for (a–c) 2 M TBA and (e and f) 0.1 M TBA. (d) The corrected absorbance spectra of pure water, 2 M TBA, and 0.1 M TBA.

To optimize the subtraction factor, it is useful to look at a small peak. As such, the free-OH stretch of non-hydrogen-bonded OH groups at ~3660 cm^{-1}, shown in Fig. 2c and f, is especially illustrative of the sensitivity of solvation shell spectroscopy. This peak originates from broken hydrogen bonds due to interactions with the hydrophobic regions of the alcohol, and is typically obscured by the much larger hydrogen-bonded OH stretch in the absorbance spectrum. At high alcohol concentrations (Fig. 2c), this peak can be a few percent of the overall absorbance and is easily observed in the solvation shell spectrum, despite noise caused by atmospheric water lines in the same frequency range. As the alcohol concentration is decreased (Fig. 2f), this peak becomes harder to distinguish and truly emphasizes the power of solvation shell spectroscopy. In the corrected ATR spectra (Fig. 2d), a 0.1 M solution of TBA is virtually indistinguishable from bulk water, while the sharp peaks of TBA can be seen clearly at a higher concentration (2 M) of the alcohol. Interestingly, solvation shell spectroscopy at high concentration is further complicated by a change in the slope of the high-frequency edge of the spectrum – at frequencies normally considered higher than the OH-stretch range, the water has an absorbance that is distinctly different than the alcohol solution and creates a slightly negative offset under the free-OH band.

MCR analysis and comparison with weighted subtraction. For comparison, the two TBA data sets analysed above were also analysed using the MCR routine. Fig. 3a shows the initial MCR result, as well as the fine-tuned rotation and the weighted subtraction result for the high-concentration data. Due to the high-frequency offset in this data, the initial result is undersubtracted, but by fine-tuning the rotation in the MCR output based on the free OH, an identical result to the weighted subtraction is obtained. The same is true for the solvation shell spectrum of 0.1 M TBA shown in Fig. 3b, which is still rather high quality despite the low concentration. While MCR is a powerful method and capable of more complex analyses, the weighted subtraction method can be applied equivalently in a wide range of applications of interest across broad fields. In the two-component limit, the two methods are equivalent. Furthermore, the MCR method

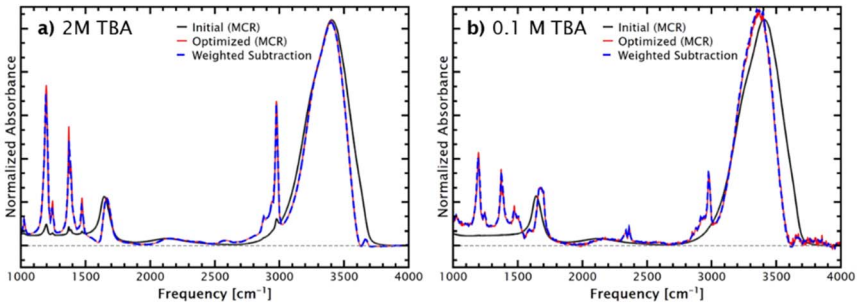

Fig. 3 The solvation shell spectrum of TBA obtained as the initial and optimized outputs from the MCR routine, as well as the direct subtraction result for (a) 2 M TBA and (b) 0.1 M TBA. After optimization, the two methods are fully equivalent for two-component systems.

can give misleading results if the initial MCR result is used as is without further refinement of the basis-set rotation, based on chemical and experimental considerations, as shown in Fig. 3. Therefore, while our initial studies used the MCR method, we now use the weighted subtraction method for its ease of use and transparent, flexible application.

Both the weighted subtraction and the MCR approach are affected by the data quality, particularly baseline offsets and interfering atmospheric absorbances, which are increasingly problematic as the solute concentration decreases. Interferences from atmospheric absorbances can cause artifacts, particularly in the OH-stretch region, and false identification of free-OH peaks, as discussed further in the SI, together with further discussion of analysing noisy data. For both methods, appropriate analysis of the solvation shell spectrum requires chemical and spectroscopic insight, and familiarity with common issues, as the rigorous mathematical application does not consider experimental noise and artifacts that are generally well-understood and can be avoided with careful application of the procedures. In all cases, reproducibility is a key factor in confidently obtaining the solvation shell spectrum. Careful analysis allows the extension of the method to increasingly complex systems and surfaces, as discussed below, starting with additives to aqueous solutions of the well-understood probe molecule TBA.

Solvation structure of TBA: from pure water to complex systems

TBA in pure water. The amphiphilic TBA solute is an illustrative example of solvation shell spectroscopy. As can be seen in the above figures, the hydrophobic part of the molecule gives rise to a distinctive "free-OH" peak around 3660 cm^{-1}. A completely free OH as found at the air–water interface has a vibrational frequency of 3700 cm^{-1}. When interacting with the hydrophobic CH_3 groups of TBA, the non-hydrogen-bonded OH vibration of the surrounding water molecules in the solvation shell is slightly shifted to 3660 cm^{-1} due to the dispersion interactions. Such free-OH peaks are a hallmark of, and a convenient marker for, normal hydrophobic surfaces.[18–21,51] However, for positively charged hydrophobic surfaces such as those found in the tetramethylammonium cation, the free OH disappears since the OH group is rotated away from the interface due to charge repulsion.[52]

In both cases, the overall solvation shell spectrum is slightly shifted to lower frequencies compared to bulk water due to the overall strengthening of the hydrogen-bonded network of water surrounding the hydrophobic residue. This tetrahedral network of water around hydrophobic patches has also been observed for flat hydrophobic surfaces in SFG spectroscopy,[53] and in THz spectroscopy of TBA in solution.[54–56] The well-studied amphiphilic TBA provides an interesting starting point for exploring more complex systems, as demonstrated below.

Ions in the solvation shell of TBA. While most solvation shell studies have focused on solutions in pure water, solutions in buffers can also be studied when care is taken to ensure that the pure solvent (in this case, a buffer solution) is identical in the solution and solvent. Whether the ion concentration in the solvation shell is different than in the bulk solvent is an interesting question, particularly relevant to the pharmaceutical industry and formulations where excipients and additives in the solvent are included to stabilize the solvation of bioactive molecules. Ben-Amotz and co-workers investigated the change in the OH stretch in the solvation shell of TBA when introducing ions into the solvent.[47] Here, we focus on the vibration of the ion itself and use solvation shell spectroscopy to quantify the amount of ions in the solvation shell compared with the bulk ion concentration.

We investigate the solvation shell of TBA in NaN_3 solutions. Fig. 4 shows the solvation shell spectra of 1.0 M TBA solutions with varying azide concentrations. Azide is a convenient ion to study because the strong vibration at 2042 cm^{-1}, which is usually clear of other interesting features in the vibrational spectrum, can be used to quantify the amount of azide in the solvation shell. Fig. 4 shows how the solvation shell spectrum changes with bulk azide concentration, and the magnitude of the azide peak in the solvation shell as a function of the bulk azide concentration. This behaviour closely resembles that of ions at the outermost layer of the air–water interface studied by resonant second-harmonic generation (SHG) spectroscopy.[57,58] Accordingly, we performed a similar Langmuir analysis of azide in the solvation shell of TBA and obtained a Gibbs free energy of adsorption of −7.6 kJ mol^{-1}. In comparison, the value obtained for the adsorption of azide to the outermost layer of the air–water interface was −10.0 kJ mol^{-1}. However, care must be taken when

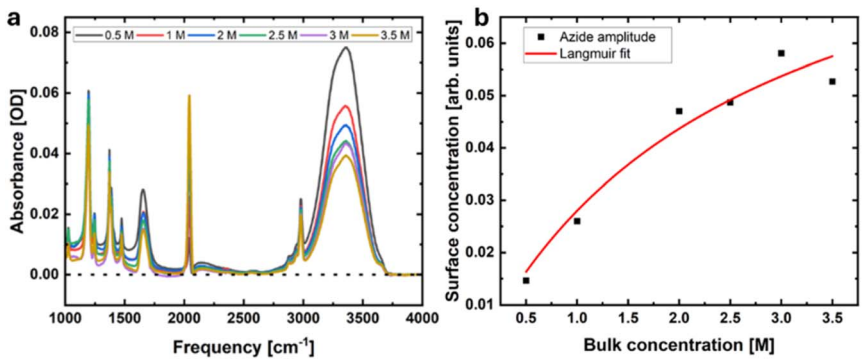

Fig. 4 Azide ions in the solvation shell of TBA: (a) the solvation shell spectra with changing azide concentration, and (b) a Langmuir fit of the azide peak amplitude as a function of azide concentration in the bulk solvent.

comparing these two values: for the air–water interface, the net adsorption through the entire interfacial layer is negative (*i.e.* an overall positive Gibbs free energy of adsorption) and only at the outermost liquid layer is there a positive absorption (negative Gibbs free energy), given the non-monotonic concentration profiles at the interface. In the present case, we are capturing the entire solvation shell, not only the layer closest to TBA. This means that in this case, there is a true net accumulation of azide ions at the TBA surface compared to the bulk.

TBA in mixed solvents. While most solvation shell studies have been performed in pure water or in buffered solutions, we recently extended IR solvation shell spectroscopy to mixed solvent systems of TBA in water/propanol solvent mixtures, across the full range from pure propanol to pure water.[41] By combining solvation shell spectroscopy with simulations, we discovered that the solvation shell of the amphiphilic TBA solute in the mixed solvent exhibits non-monotonic dependences on the solvent composition and thus provides a molecular probe of the non-ideal mixing behaviour of the solvents. Furthermore, we found that the solvation shells of an amphiphilic solute display hydrophilic-hydrophobic bilayers and multilayers of the solvent molecules depending on the solvent mixture, similar to electric double layers at flat interfaces. This example illustrates that solvation shell spectroscopy can be applied not only to pure water or salt solutions but also to more complex solvent mixtures to probe their non-ideal mixing behaviour at the molecular level. It also illustrates the power of combining solvation shell spectroscopy with simulations to obtain a detailed molecular picture of the local solvation structure.

Hydration energies – hydrogen-bond strength. The qualitative interpretation of aqueous solvation shell spectra relies on the correlation between the OH-stretch frequency and the hydrogen-bond strength. As such, this correlation offers a straightforward qualitative interpretation of the spectra. If the solvation shell spectra are shifted to higher frequencies than bulk water, it means that the hydrogen-bonding interactions in the solvation shell are weaker than in bulk water, and if the solvation shell spectrum is shifted to lower frequencies, then the hydrogen-bonding interactions are stronger than in bulk water. Of particular note is the free OH, found as a relatively sharp peak around 3650–3700 cm^{-1}, depending on the van der Waals interactions, which is a hallmark of water in hydrophobic environments that is unable to form all of its hydrogen bonds. Given the unique assignment and identification of this peak, it can be easily interpreted and has been used to shed light on the nature of hydrophobic interactions.[18–21]

The straightforward qualitative interpretation of solvation shell spectra offers great insight into the general intermolecular interactions between solute and solvent. However, it can be advantageous to further quantify these interactions. With increasing hydrogen-bond strength, the OH-stretch potential widens, thereby shifting the vibration to lower frequencies. Theory offers a direct translation of the OH-stretch frequency to hydrogen-bond strength *via* a linear relation over the typical water OH frequency range from 3000 to 3700 cm^{-1}:[1]

$$\text{HB strength: } \Delta E_{D\rightarrow A}\ (\text{kJ mol}^{-1}) = 0.0392 \times \omega\ (\text{cm}^{-1}) - 150.6$$

Given that the peak width also broadens as a function of hydrogen-bond strength, this direct linear relationship should be taken only as an approximation,

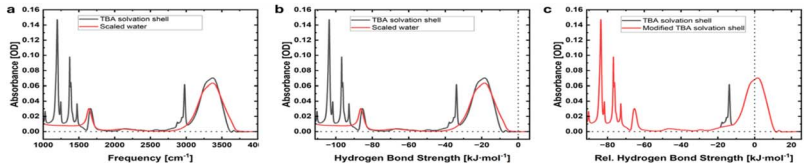

Fig. 5 Calculation of the average hydration energy in the solvation shell of 2 M TBA. (a) The solvation shell spectrum as a function of frequency, which is then (b) converted to the absolute hydrogen-bond strength, and (c) the relative hydrogen-bond strength compared to the average of bulk water.

but it works to quantify the average hydrogen-bond interactions. Using this direct relationship, the OH-stretch spectrum can be converted into a distribution of hydrogen-bond interactions, as illustrated in Fig. 5. What is relevant is how the hydrogen-bond interactions in the solvation shell compare to those of bulk water. This can be quantified by shifting the hydrogen-bond strength from the absolute value to the change relative to the average of bulk water. Accordingly, OH-stretch vibrations at higher frequencies contribute to a net weaker hydrogen-bond network and OH vibrations at lower frequencies contribute to a net stronger hydrogen-bond network in the solvation shell compared with that of bulk water. The average hydrogen-bond interaction in the solvation shell is then simply found as the average of the hydrogen-bond distribution relative to bulk water. If there is spectral overlap of the OH-stretch band of water in the solvation shell with CH stretches, these must be subtracted before the average is taken, as also illustrated in Fig. 5c. For the example shown in Fig. 5 of 2 M TBA, the average hydrogen-bond strength in the solvation shell is found to be 1.56 kJ mol^{-1} stronger than the average hydrogen-bond interactions in bulk water when averaged from 2500 to 4000 cm^{-1}. Here it should be noted that the oscillator strength of the OH stretch in the IR also varies as a function of the OH-stretch frequency. For small shifts of the OH-stretch spectrum, this effect is minor, but for larger shifts this should be taken into account, which can be done using another theory-derived average relationship between the transition dipole moment and the OH-stretch frequency.[1] While a lot of information can be derived from the qualitative interpretation, this quantification is useful for comparing to other measurements, such as atomic force measurements.[42]

Biomolecules

Solvation shell spectroscopy can provide insight not only into small organic or inorganic compounds, but is also valuable for understanding the hydration of biomolecules, such as proteins or lipids. In our first publication introducing IR solvation shell spectroscopy, we quantified the amount of water in the solvation shell of an anti-freeze protein.[39] In our experience, high-quality solvation shell spectra can be obtained with protein concentrations of a few mg ml^{-1} and above. In a recent investigation, we compared the solvation shell of halophilic proteins to mesophilic (normal) proteins as a function of salt concentration, combined with molecular dynamics simulations. As halophilic proteins typically contain a higher density of acidic side chains compared to mesophilic proteins, it had been suggested that these acidic side chains were necessary to keep the protein hydrated at high salt concentrations. However, we found no distinguishable difference in the hydration of

halophilic proteins and mesophilic proteins at high salt concentrations, suggesting a different evolutionary drive for the increased amount of acidic side chains in halophilic proteins. These studies were performed with a protein concentration of 0.5 mg ml^{-1}, which is pushing the current noise limit of solvation shell spectroscopy of proteins, and again highlight the power of combining solvation shell spectroscopy with simulations to obtain a detailed molecular picture of solvation.[40] This push to lower concentration is critical for applying solvation shell spectroscopy to custom-synthesized biomolecules that can only be made in limiting amounts. Furthermore, pushing the method to lower S/N systems allows for studying even large objects, such as the meso- and macroscopic systems discussed below.

Meso- and macroscopic surfaces

By far, most solvation shell studies have focused on solutions of small molecules or biomolecules. However, the same principle can be applied to larger objects, as recently demonstrated on 900 nm diameter polystyrene beads and membrane surfaces.[42] For these mesoscale objects, the surface-to-volume ratio is smaller compared to molecules, giving rise to further challenges in the signal-to-noise ratio, since the solvation shell spectrum is less than a percent of the total spectrum. However, when the measurements are taken with care, reliable spectra can still be obtained. For the case of polystyrene beads, the solvation shell spectra are of surprisingly good quality given the low concentration of the polystyrene beads in the solution, 1 mg ml^{-1}. However, comparing the magnitude of the CH-stretch vibration of the polystyrene bead solution on the ATR crystal to a bulk film of polystyrene reveals that the beads accumulate on the ATR crystal to form a nearly close-packed layer, as illustrated in Fig. 6. More specifically, the absorption of the 2850 cm^{-1} CH vibration of a 40 μm-thick polystyrene film is ∼1, while that of the solution on the ATR crystal is 0.00042. Accounting for the effective penetration depth of ∼188 nm of the ATR/solution interface, this corresponds to an effective thickness of 44 nm of polystyrene on the ATR crystal. Assuming that the beads are spheres lying on the ATR crystal, this in turn corresponds to roughly a third of a full packed monolayer of beads on the ATR crystal. This up-concentration of beads on the ATR crystal compared to the bulk solution explains the surprisingly good quality of the obtained solvation shell spectra and opens up a multitude of applications for studying solvation of functionalized mesoscale objects.

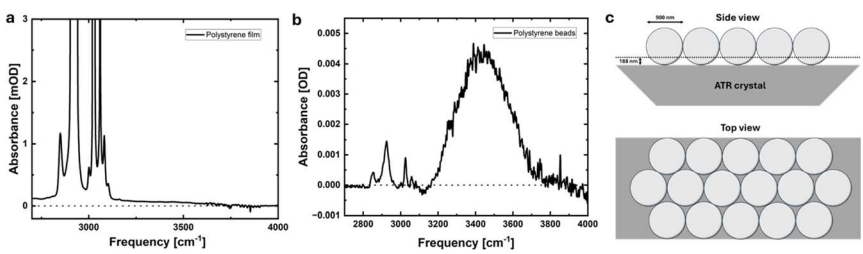

Fig. 6 Solvation shell spectroscopy of 900 nm polystyrene beads forming a packed monolayer on the ATR crystal. (a) The absorption spectrum of a 40 μm-thick polystyrene film, compared with (b) the solvation shell spectrum of 900 nm diameter polystyrene beads. (c) A schematic showing the polystyrene beads forming a close-packed layer on the ATR crystal.

As a further extension of the method, we applied it to functionalized membrane surfaces, where we observed that the solvation shell spectra of the membranes indeed change with surface functionalization and buffer conditions, which can be further quantified in terms of hydrogen-bond strength, as described above, and compared to other experiments.[42] Here we note that a similar approach has been used recently to investigate solvent interactions with other flat surfaces, such as gold functionalized with self-assembled monolayers.[59] That solvation shell spectroscopy can be sensitive enough to measure the solvent interacting with nominally flat surfaces greatly broadens the applicability of the method and could potentially complement truly surface-specific spectroscopies such as SFG, given the differences in selection rules and sensitivities.

Conclusions

IR solvation shell spectroscopy is a powerful emerging method, providing direct spectroscopic characterization of the interactions between solute and solvent. In its simplicity, it can be widely used to study interactions at the solute–solvent interface in a multitude of systems encompassing not only small molecules and biomolecules, but also larger meso- and macroscopic objects, such as beads and surfaces. Here we aim to give a comprehensive description of the method, including common pitfalls and how to obtain reliable spectra to broaden the usability of the method. When implemented with care, IR solvation shell spectroscopy can provide key molecular insight into solute–solvent interactions to uncover the driving forces for solvation that are difficult to obtain by other experimental means.

Specifically, we used the well-studied TBA molecule to demonstrate several advances in IR solvation shell spectroscopy. Reducing the necessary signal-to-noise ratio allows the method to be applied to molecular interfaces at low concentrations, such as those required for scarce samples, as well as at flat or complex surfaces where the number of surface molecules is low. Furthermore, the solvation shell spectra of simple and complex systems can be carefully analyzed to extract quantitative chemical information, such as adsorption and hydration energies. As such, we determined the Gibbs free energy of adsorption of azide ions to the solvation shell of TBA to be -7.6 kJ mol^{-1}, in comparison to -10.0 kJ mol^{-1} obtained for the adsorption of azide to the outermost layer of the air–water interface.[57,58] Furthermore, we quantified the average hydrogen-bond strength in the solvation shell of TBA in pure water to be 1.56 kJ mol^{-1} stronger than the average hydrogen-bond interactions within bulk water.

Combined with theoretical simulations, solvation shell spectroscopy is a particularly powerful combination to provide molecular insight into solute–solvent interactions critical for a number of applications spanning fundamental interactions behind the hydrophobic effect, non-ideal mixtures, biomolecular solvation and interactions, and formulations. This breadth of examples demonstrates the diverse potential of solvation shell spectroscopy – with careful consideration, this powerful method can be applied to study solvent interactions in practically any system, from small molecules, biomolecules, and complex solvents, to even mesoscopic and macroscopic interfaces.

Author contributions

Conceptualization P. B. P.; methodology D. K. H., P. B. P.; validation B. M., L. N. A.; formal analysis A. M. S., B. M., L. N. A., P. B. P.; investigation B. M., L. N. A.; resources P. B. P.; writing – original draft A. M. S., B. M., D. K. H., P. B. P.; writing – review & editing A. M. S., B. M., D. K. H., P. B. P.; visualization A. M. S., B. M., D. K. H., P. B. P.; supervision P. B. P.; project administration P. B. P.; funding acquisition P. B. P., D. K. H.

Conflicts of interest

There are no conflicts to declare.

Data availability

Data for this article, including spectroscopic data, are available at the RESOLV data repository at https://doi.org/10.17877/RESOLV-2026-3CYRV3.

Supplementary information (SI): further discussion of theoretical and experimental considerations for solvation shell spectroscopy. See DOI: https://doi.org/10.1039/d5fd00156k.

Acknowledgements

This work was financed by the Deutsche Forschungsgemeinschaft (DFG, German Research Foundation) under Germany's Excellence Strategy EXC2033, project number 390677874 ("RESOLV") and GRK2376, project number 331085229 ("Confinement-Controlled Chemistry"), as well as the Natural Sciences and Engineering Research Council of Canada, project number RGPIN-2020-06030.

Notes and references

1 D. Ojha, K. Karhan and T. D. Kühne, *Sci. Rep.*, 2018, **8**, 16888.
2 S. A. Corcelli and J. L. Skinner, *J. Phys. Chem. A*, 2005, **109**, 6154–6165.
3 J. J. Loparo, S. T. Roberts, R. a. Nicodemus and A. Tokmakoff, *Chem. Phys.*, 2007, **341**, 218–229.
4 Y. R. Shen, *The Principles of Nonlinear Optics*, John Wiley & Sons, Inc., New York, 1984.
5 F. Perakis, L. De Marco, A. Shalit, F. Tang, Z. R. Kann, T. D. Kühne, R. Torre, M. Bonn and Y. Nagata, *Chem. Rev.*, 2016, **116**, 7590–7607.
6 S. E. Sanders, H. Vanselous and P. B. Petersen, *J. Phys.: Condens. Matter*, 2018, **30**, 113001.
7 S. Roy and D. K. Hore, *J. Phys. Chem. C*, 2012, **116**(43), 22867–22877.
8 Y. C. Wen, S. Zha, X. Liu, S. Yang, P. Guo, G. Shi, H. Fang, Y. R. Shen and C. Tian, *Phys. Rev. Lett.*, 2016, **116**, 016101.
9 S. Nihonyanagi, S. Yamaguchi and T. Tahara, *Chem. Rev.*, 2017, **117**, 10665–10693.
10 M. L. McDermott, H. Vanselous, S. A. Corcelli and P. B. Petersen, *ACS Cent. Sci.*, 2017, **3**, 708–714.
11 E. C. Y. Yan, L. Fu, Z. Wang and W. Liu, *Chem. Rev.*, 2014, **114**, 8471–8498.

12 S. Roke and G. Gonella, *Annu. Rev. Phys. Chem.*, 2012, **63**, 353–378.
13 R. Scheu, Y. Chen, H. B. De Aguiar, B. M. Rankin, D. Ben-Amotz and S. Roke, *J. Am. Chem. Soc.*, 2014, **136**, 2040–2047.
14 J. Grdadolnik, *Vib. Spectrosc.*, 2003, **31**, 279–288.
15 J. Grdadolnik and Y. Marechal, *Biopolymers*, 2001, **62**, 40–53.
16 Y. Maréchal, *J. Mol. Struct.*, 1997, **416**, 133–143.
17 I. A. Mudunkotuwa, A. Al Minshid and V. H. Grassian, *Analyst*, 2014, **139**, 870–881.
18 P. Perera, M. Wyche, Y. Loethen and D. Ben-Amotz, *J. Am. Chem. Soc.*, 2008, **130**, 4576–4577.
19 P. N. Perera, K. R. Fega, C. Lawrence, E. J. Sundstrom, J. Tomlinson-Phillips and D. Ben-Amotz, *Proc. Natl. Acad. Sci. U. S. A.*, 2009, **106**, 12230–12234.
20 J. G. Davis, K. P. Gierszal, P. Wang and D. Ben-Amotz, *Nature*, 2012, **491**, 582–585.
21 D. Ben-Amotz, *J. Am. Chem. Soc.*, 2019, **141**, 10569–10580.
22 M. Ahmed, A. K. Singh and J. A. Mondal, *Phys. Chem. Chem. Phys.*, 2016, **18**, 2767–2775.
23 Y. Shen, B. Liu, J. Cui, J. Xiang, M. Liu, Y. Han and Y. Wang, *J. Phys. Chem. Lett.*, 2020, **11**, 7429–7437.
24 S. Saha, S. Roy, P. Mathi and J. A. Mondal, *J. Phys. Chem. A*, 2019, **123**, 2924–2934.
25 L. Zhang, T. Cambron, Y. Niu, Z. Xu, N. Su, H. Zheng, K. Wei and P. Ray, *Anal. Chem.*, 2019, **91**, 2784–2790.
26 Y. H. Wang, S. Zheng, W. M. Yang, R. Y. Zhou, Q. F. He, P. Radjenovic, J. C. Dong, S. Li, J. Zheng, Z. L. Yang, G. Attard, F. Pan, Z. Q. Tian and J. F. Li, *Nature*, 2021, **600**, 81–85.
27 M. Ahmed, V. Namboodiri, A. K. Singh, J. A. Mondal and S. K. Sarkar, *J. Phys. Chem. B*, 2013, **117**, 16479–16485.
28 M. Ahmed, V. Namboodiri, P. Mathi, A. K. Singh and J. A. Mondal, *J. Phys. Chem. C*, 2016, **120**, 10252–10260.
29 B. A. Rogers, H. I. Okur, C. Yan, T. Yang, J. Heyda and P. S. Cremer, *Nat. Chem.*, 2022, **14**, 40–45.
30 T. Mukherjee, E. K. Smith, M. Sulpizi and M. Rabe, *Nanoscale*, 2025, **17**, 15772–15784.
31 S. Z. Zou, Y. X. Chen, B. W. Mao, B. Ren and Z. Q. Tian, *J. Electroanal. Chem.*, 1997, **424**, 19–24.
32 K. I. Ataka, T. Yotsuyanagi and M. Osawa, *J. Phys. Chem.*, 1996, **100**, 10664–10672.
33 M. Osawa, M. Tsushima, H. Mogami, G. Samjeské and A. Yamakata, *J. Phys. Chem. C*, 2008, **112**, 4248–4256.
34 M. Grossutti, J. J. Leitch, R. Seenath, M. Karaskiewicz and J. Lipkowski, *Langmuir*, 2015, **31**, 4411–4418.
35 B. Chen, M. Wijesinghe, Y.-S. Hsu, R. Zhang, C. Gunathunge, A. Grimaud and M. Waegele, *ChemRxiv*, 2025, preprint, DOI: 10.26434/chemrxiv-2025-zdbxg.
36 C. Y. Li, J. B. Le, Y. H. Wang, S. Chen, Z. L. Yang, J. F. Li, J. Cheng and Z. Q. Tian, *Nat. Mater.*, 2019, **18**, 697–701.
37 C. Y. Li, M. Chen, S. Liu, X. Lu, J. Meng, J. Yan, H. D. Abruña, G. Feng and T. Lian, *Nat. Commun.*, 2022, **13**, 5330.

38 L. K. S. Bonagiri, D. M. Arvelo, F. Zhao, J. Kim, Q. Ai, S. Zhou, K. S. Panse, R. Garcia and Y. Zhang, *Nat. Commun.*, 2026, **17**, 2230, DOI: 10.1038/s41467-026-68667-y.
39 Y. Sun and P. B. Petersen, *J. Phys. Chem. Lett.*, 2017, **8**, 611–614.
40 H. Geraili Daronkola, B. Moussa, Ó. Millet, O. Krenczyk, G. Ortega-Quintanilla, P. B. Petersen and A. Vila Verde, *Protein Sci.*, 2025, **34**, e5241.
41 E. Casalini, A. M. Stingel, B. Moussa, M. Personeni, P. B. Petersen and A. Vila Verde, *JACS Au*, 2025, **5**, 2992–2999.
42 S. Karla, M. Sorci, B. Moussa, R. Banik, P. B. Petersen, J. Plawsky and G. Belfort, *J. Colloid Interface Sci.*, 2026, **701**, 138530.
43 A. Novak, in *Large Molecules. Structure and Bonding*, Springer, Berlin, Heidelberg, 1974, vol. 18, pp. 177–216.
44 C. A. Daly, L. M. Streacker, Y. Sun, S. R. Pattenaude, A. A. Hassanali, P. B. Petersen, S. A. Corcelli and D. Ben-Amotz, *J. Phys. Chem. Lett.*, 2017, **8**, 5246–5252.
45 C. I. Drexler, T. C. Miller, B. A. Rogers, Y. C. Li, C. A. Daly, T. Yang, S. A. Corcelli and P. S. Cremer, *J. Am. Chem. Soc.*, 2019, **141**, 6930–6936.
46 K. P. Gierszal, J. G. Davis, M. D. Hands, D. S. Wilcox, L. V Slipchenko and D. Ben-Amotz, *J. Phys. Chem. Lett.*, 2011, **2**, 2930–2933.
47 B. M. Rankin, M. D. Hands, D. S. Wilcox, K. R. Fega, L. V. Slipchenko and D. Ben-Amotz, *Faraday Discuss.*, 2013, **160**, 255–270.
48 D. S. Wilcox, B. M. Rankin and D. Ben-Amotz, *Faraday Discuss.*, 2013, **167**, 177–190.
49 B. M. Rankin, D. Ben-Amotz, S. T. van der Post and H. J. Bakker, *J. Phys. Chem. Lett.*, 2015, **6**, 688–692.
50 A. J. Bredt and D. Ben-Amotz, *Phys. Chem. Chem. Phys.*, 2020, **22**, 11724–11730.
51 J. R. Robalo, D. Mendes De Oliveira, P. Imhof, D. Ben-Amotz and A. Vila Verde, *Phys. Chem. Chem. Phys.*, 2020, **22**, 22997–23008.
52 N. Ghosh, S. Roy, A. Bandyopadhyay and J. A. Mondal, *Liquids*, 2023, **3**, 19–39.
53 W. Chen, S. E. Sanders, B. Özdamar, D. Louaas, F. S. Brigiano, S. Pezzotti, P. B. Petersen and M.-P. Gaigeot, *J. Phys. Chem. Lett.*, 2023, **14**, 1301–1309.
54 S. Pezzotti, F. Sebastiani, E. P. van Dam, S. Ramos, V. Conti Nibali, G. Schwaab and M. Havenith, *Angew. Chem., Int. Ed.*, 2022, **61**, e202203893.
55 V. Conti Nibali, S. Pezzotti, F. Sebastiani, D. R. Galimberti, G. Schwaab, M. Heyden, M. P. Gaigeot and M. Havenith, *J. Phys. Chem. Lett.*, 2020, **11**, 4809–4816.
56 S. Pezzotti, A. Serva, F. Sebastiani, F. S. Brigiano, D. R. Galimberti, L. Potier, S. Alfarano, G. Schwaab, M. Havenith and M.-P. Gaigeot, *J. Phys. Chem. Lett.*, 2021, **12**, 3827–3836.
57 P. B. Petersen, *Surface Structure of Aqueous Electrolyte Solutions Probed by UV Second Harmonic Generation*, PhD thesis, UC Berkeley, 2005.
58 P. B. Petersen and R. J. Saykally, *Annu. Rev. Phys. Chem.*, 2006, **57**, 333–364.
59 S. Maeda, S. Chikami, S. Song, M. V. Balois-Oguchi, A. Katase, G. V. Latag, T. Tanaka and T. Hayashi, *Anal. Chem.*, 2025, **97**, 20156–20163.